ChemCatChem

Research Article
doi.org/10.1002/cctc.202401913

Chemistry Europe
European Chemical Societies Publishing

www.chemcatchem.org

Stabilization of Ru-Core Pt-Shell Model Electrodes by Electronic Effects and Electrooxidation Reactions

Albert K. Engstfeld[+],*[a] Lukas Forschner[+],[a] Mario Löw[++],[a] Linus Pithan[+++],[b] Paul Beyer[++++],[b] Zenonas Jusys[+++++,++++++],[a] Joachim Bansmann,[a] R. Jürgen Behm[++],*[a] and Jakub Drnec[b]

The technical application of bimetallic core-shell particles, which are highly attractive because of their high electrocatalytic activity, depends crucially on their long-term stability under operating conditions. In the present multi-method study, we explored the stability of structurally well-defined Ru-core Pt-shell model systems during the CO oxidation (COOR) and methanol oxidation (MOR) reactions. These electrodes consist of a single-crystalline Ru(0001) substrate covered by epitaxial Pt films of one to three atomic layers. The reaction-induced modifications in the surface morphology were identified by scanning tunneling microscopy (STM) measurements performed before and after the electrocatalytic measurement, which reveal a higher stability for electrodes with around three layers of Pt (up to 1.4 V vs. the reversible hydrogen electrode) than for those with fewer layers. Differential electrochemical mass spectrometry (DEMS) measurements carried out during the COOR allow separation of the COOR currents from surface redox processes, providing insight into the role of surface oxidation / reduction processes during the COOR. *Operando* surface X-ray diffraction (SXRD) measurements performed during electro-oxidation of methanol confirm the much higher stability of the electrodes with three Pt layers. The main conclusion of this work is that during the electro-oxidation of organic molecules, the stability of the electrodes is, in general, improved due to the reactive removal of OH/O species from the surface.

1. Introduction

Metal-based core-shell catalysts consist of a thin mono- or multilayer metal film covering a different metal core. Selectively changing the shell thickness, the particle size, or the composition of the core (alloying) or the shell, results in changes in the electronic properties of the surface atoms, which in turn has a significant impact on their catalytic activity.[1–8] Prominent examples are Pt-modified Ru-core nanoparticle catalysts, which were intensively studied over the last decade for the oxygen reduction reaction (ORR),[9–13] the hydrogen oxidation reaction (HOR) including also the CO tolerance in that reaction,[10,14–18] the hydrogen evolution reaction (HER),[17,18] the formic acid oxidation reaction (FAOR),[19] the ethanol oxidation reaction (EOR),[20–23] the carbon monoxide oxidation reaction (COOR),[11,19] or the methanol oxidation reaction (MOR).[21,24–29]

An important aspect for possible applications of such electrodes is their stability during operation. For Pt–Ru nanoparticles, this includes, in particular, the dissolution of the individual components into the electrolyte, where Ru dissolution is more facile than Pt, but also a possible surface restructuring. [30–35] For Ru-core Pt-shell nanoparticles it was shown that the Pt shell slows down or even inhibits the dissolution of Ru, and the effect is usually stronger with increasing Pt layer thickness.[10,13,14,30,36,37] Nevertheless, Ru dissolution often occurred also for these materials during long-term stability tests, which was attributed to the formation of pinholes in the Pt shell.[38]

Fundamental studies aiming at a more detailed understanding of the reactivity, adsorption properties, and stability of Ru–Pt core-shell catalyst often use Pt-modified Ru(0001) electrodes.[39–50] These model systems are atomically flat, structurally, and chemically well-defined and therefore well suited for fundamental studies, including comparison of theory and experiment.[6,39] Model studies using such electrodes in the

[a] *A. K. Engstfeld[+], L. Forschner[+], M. Löw[++], Z. Jusys[+++++,++++++], J. Bansmann, R. J. Behm[++]*
Institute of Surface Chemistry and Catalysis, Ulm University D-89069, Ulm, Germany
E-mail: albert.engstfeld@uni-ulm.de
juergen.behm@uni-ulm.de

[b] *L. Pithan[+++], P. Beyer[++++], J. Drnec*
ESRF: Experimental division, ESRF, Grenoble F-38000, France

***Abbreviations**: CO electro-oxidation, carbon monoxide electro-oxidation; core-shell particles; CV, cyclic voltammogram; DEMS, Differential electrochemical mass spectrometry; electrocatalysis; MeOH, methanol electro-oxidation; SXRD, surface X-ray diffraction*

[+] *Institute of Electrochemistry, Ulm University, D-89069 Ulm, Germany*
[++] *Institute of Theoretical Chemistry, D-89081 Ulm, Germany*
[+++] *Deutsches Elektronen-Synchrotron DESY, Notkestraße 85, 22607 Hamburg, Germany*
[++++] *Fachbereich Physik, Freie Universität Berlin, D-14195 Berlin, Germany*
[+++++] *Helmholtz Institute Ulm Electrochemical Energy Storage (HIU), Ulm, Germany*
[++++++] *Present Address: Karlsruhe Institute of Technology (KIT), D-76021, Karlsruhe, Germany*

Supporting information for this article is available on the WWW under https://doi.org/10.1002/cctc.202401913

ORR,[51] the hydrogen underpotential deposition (HUPD),[41] or the MOR[45,52] revealed a distinct influence of the Pt layer thickness. The stability of such model electrodes has been investigated so far only for oxidation reactions on (sub-) monolayer Pt film-covered surfaces, employing ultrahigh vacuum (UHV) scanning tunneling microscopy (STM) measurements before and after the electrochemical/-catalytic measurements.[53–55] The results indicated that Pt protects the low-coordinated Ru atoms at step edges against dissolution, shifting the onset potential for Ru dissolution to more positive values. For potentials larger than 1.05 V, Ru dissolution on the Pt-modified Ru(0001) electrodes was mainly observed at the Ru steps (step flow corrosion). Furthermore, Pt was found to restructure, forming Pt clusters on the surface in the regions of the original Pt islands.

In this work, we focus on the stability of atomically flat, single-crystalline Ru(0001) electrodes, whose surface is modified by Pt films with Pt thicknesses of up to four layers during the electro-oxidation of methanol (MeOH) and CO in acid at potentials larger than 1.05 V, and the impact of any structural modifications on the activity of these samples on the COOR. This potential had been chosen as upper potential limit in previous studies to prevent possible restructuring of the electrodes during the experiment.[41,51,52] In the present work, we first studied the stability and structural modifications of an electrode with three Pt layers in pure supporting H_2SO_4 electrolyte and during the MOR by surface X-ray diffraction (SXRD) at the synchrotron. The measurements indicated that these electrodes are surprisingly stable up to 1.4 V, in contrast to the submonolayer Pt modified Ru(0001) electrodes studied previously,[53–55] or to pure Pt(111) electrodes.[56–60] Inspired by this finding, we then explored the stability of Pt-modified Ru(0001) electrodes with a Pt thickness of one and three layers for the COOR. For these measurements, we chose the COOR instead of the MOR since

1. the MOR usually shows deactivation, and effects due to structural changes cannot be discerned from poisoning effects,[52]
2. the COOR is a very structure sensitive reaction for these types of electrodes,[53–55,61,62] and
3. during the COOR, only a single product is formed, which can be detected by differential electrochemical mass spectrometry (DEMS),[63] allowing us to disentangle surface redox processes from the actual COOR.

In the following, we will first present and discuss our results on the stability of Ru(0001) electrodes modified with one and three Pt layers during the COOR, including STM images recorded before and after the COOR. These results are then used to substantiate the findings in *operando* SXRD-MOR measurements on similar electrodes. We will demonstrate that the electro-oxidation of organic species can indeed improve the stability of the electrodes.

2. Results and Discussion

2.1. STM – Electrode Stability

Ru(0001) electrodes modified by a single (Pt-1) or 3.5 monolayers (ML) of Pt (Pt-3) were prepared according to previously reported approaches[41,49,52,55] (see also the Experimental Section) and characterized by STM imaging under UHV conditions. Schematic illustrations of the surface cross-section and representative STM images of the as-prepared Pt-1 and Pt-3 electrodes are shown in Figures 1a,b,c and d, respectively. As illustrated by these images, the Pt film does not grow in a perfect layer-by-layer fashion due to kinetic limitations.[39,41,49,61] It is important to note that by comparison with STM images recorded on a large set of samples with different Pt coverages, which were prepared via the same experimental procedure on different Ru(0001) substrates,[39–42,44,46,47,49–55] we verified that the distribution of Pt layer thicknesses deduced from the STM images in Figures 1c,d is representative for samples with Pt coverages of 1.0 and 3.5 ML. Therefore, they represent the macroscopic Pt layer composition of the Pt-1 and Pt-3 electrodes used in CV and SXRD measurements. On the Pt-1 electrode, the film consists of mono- and bilayer islands, exposing also the Ru(0001) substrate. The Pt-3 electrode consists of regions with two to four Pt layers and a few small five-layer islands. Bare Ru areas are no longer present after depositing more than 1.5 ML of Pt for the experimental parameters used here. Platinum layer thickness distributions are provided in the experimental Section. Figure 1e,f show representative STM images of the electrode surfaces recorded under UHV conditions after exposing the electrodes to potential cycles up to 1.35 V during the COOR (see Figure 2).

After the potential cycling up to 1.35 V in CO saturated 0.5 M H_2SO_4 (see electrocatalytic measurements below), the Pt-1 surface shows a distinct restructuring (Figure 1e), in agreement with results in previous studies.[53–55] Note that by restructuring, we refer to an observable change in surface structure and morphology in general, without necessarily knowing about the exact atomic arrangement of the atoms after the restructuring process in the respective regions. This includes holes in the monolayer film and the Ru(0001) substrate at the former Ru step (marked by an arrow). Interestingly, the restructuring of the bilayer Pt film areas (marked by dashed circles) seems much more pronounced than that of the monolayer areas, which will be discussed below. One possibility for hole formation is the dissolution of material in the electrolyte as ions or oxidized species, which is known to occur for both pure Pt and Ru during the positive- and/or negative-going scan in a complete potential cycle, in particular in the potential region for surface oxide formation and reduction. This is reflected in Pourbaix diagrams,[31,32] and dissolution of Pt and Ru was directly demonstrated also by inductively-coupled plasma mass spectrometry (ICP-MS) measurements.[33,57,58,64] Previously, we have shown that the bare Ru(0001) is stable up to 0.9 V in this electrolyte, but not up to 1.05 V, where significant restructuring of the step edges was observed.[53,54] We suggested that dissolution is the main process behind the observed structural changes. For Pt, possible dissolution processes are not as clear, and we will show later that for electrodes that appear stable based on STM imaging performed before and after the electrochemical measurements, dissolution is probably unlikely.

The Pt-3 electrode (Figure 1f), in turn, remains almost unchanged during / after the COOR, i.e., it is highly stable under reaction conditions. This result is somewhat unexpected,

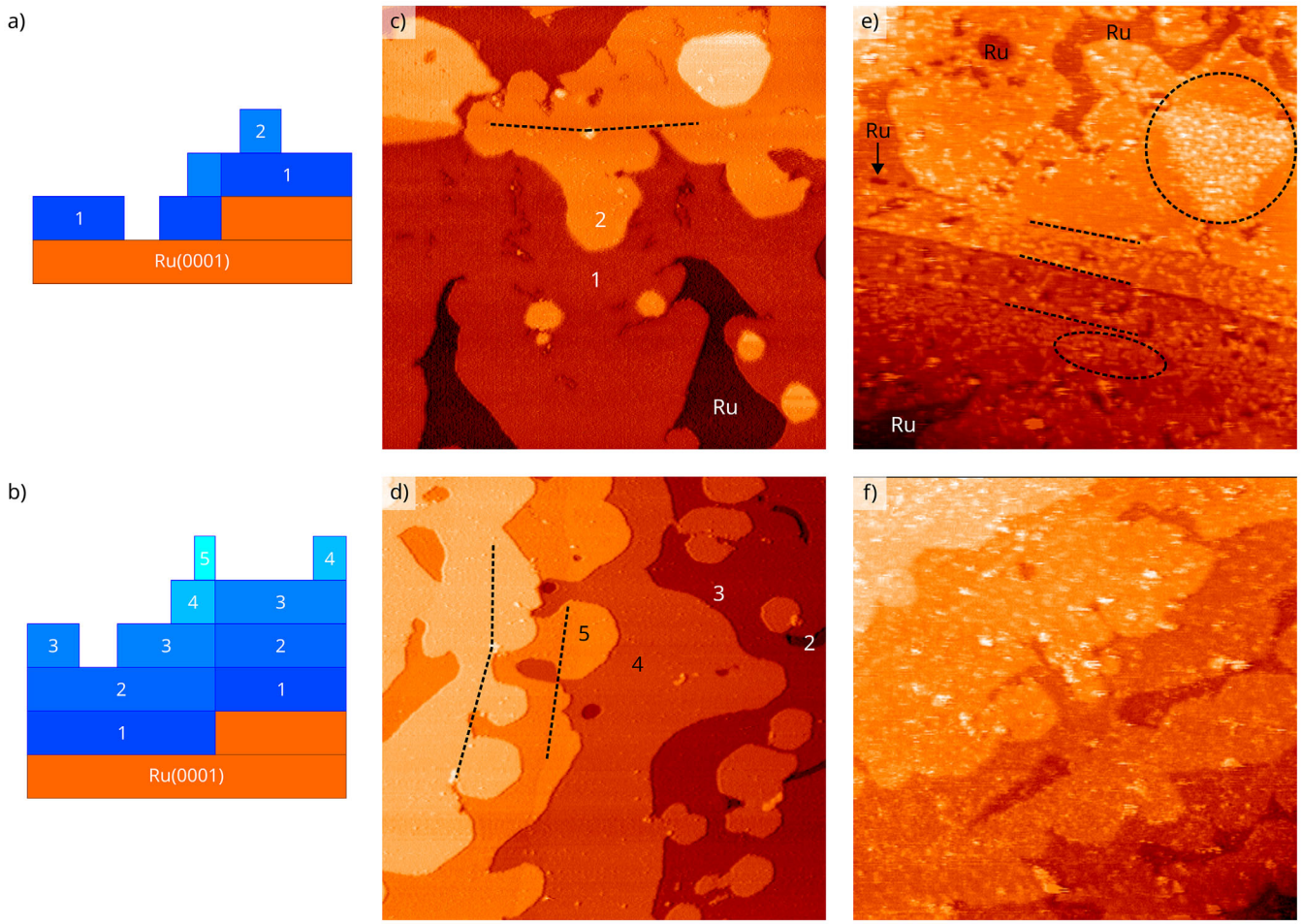

Figure 1. Schematic side view sketch of the (a) Pt-1 and (b) Pt-3 electrode. STM images of Pt-1 and Pt-3 electrodes, where (c,d) show the as prepared surface and (e,f) show the surface after the electrochemical investigation shown in Figure 2. Dashed lines mark the former Ru(0001) steps, and numbers indicate the Pt layer thickness in different regions. Regions showing the Ru substrate are marked by Ru. In (e), the location marked with an arrow shows the onset of the Ru(0001) substrate corrosion, and the dashed circles indicate regions where second layer islands are significantly restructured. All images show a region of 200 nm×200 nm.

considering that exposure of bare Pt(111) electrodes to potential cycles in CO-free electrolytes with a potential limit larger than 1.17 V leads to significant irreversible restructuring of the electrode after a few potential cycles.[56–60] Inevitably, this leads to a small increase in electrochemical active surface area. Additional STM measurements for Pt-3 electrodes restructured in a controlled way by consecutive potential cycles in pure 0.5 M H_2SO_4 are shown in Figure S1 in the Supporting Information (SI). Under these conditions, the electrochemical data suggested that the surface restructured at around 1.3 V. STM images revealed that thicker Pt layers (three atomic layers or more) remained unchanged, while the remaining regions with mono- or bilayer Pt films were entirely restructured. Reasons for the layer-dependent stability (first to third layer) are discussed below.

2.2. COOR – DEMS

The COOR on the Pt-modified Ru(0001) electrodes was characterized by cyclic voltammetry at a scan rate of 50 mVs^{-1} in CO-saturated 0.5 M H_2SO_4. The measurements were performed in a dual thin-layer electrochemical flow cell coupled with a DEMS set-up, allowing for *operando* CO_2 (m/z=44) product detection.[65] During the COOR measurements, the upper potential limit (UPL) was gradually increased in steps of 0.05 V, recording two potential cycles for each UPL. For better identification of differences, we only show a single potential cycle for UPLs of 1.05 and 1.35 V in Figure 2, respectively, for the Pt-1 electrode (left column) and the Pt-3 electrode (right column). Details of the experimental procedure and the respective parameters can be found in the Experimental Section and in the SI in Section S2, which also includes data for additional UPLs not shown here. The COOR-CVs are shown in black in Figure 2a,b. The mass spectrometric ion current of the CO_2 product formation is converted into a Faraday current and normalized to the Faraday current recorded in the COOR-CV. A detailed description of the conversion and normalization procedure and the data evaluation is provided in the SI in Section S3. The resulting curves are denoted as mass spectrometric cyclic voltammograms (MS-CVs), and are depicted in red in Figure 2c,d. For direct comparison, the COOR-CVs and MS-CVs are plotted on top of each other in Figure 2e,f. Since only CO_2 is formed during the COOR,

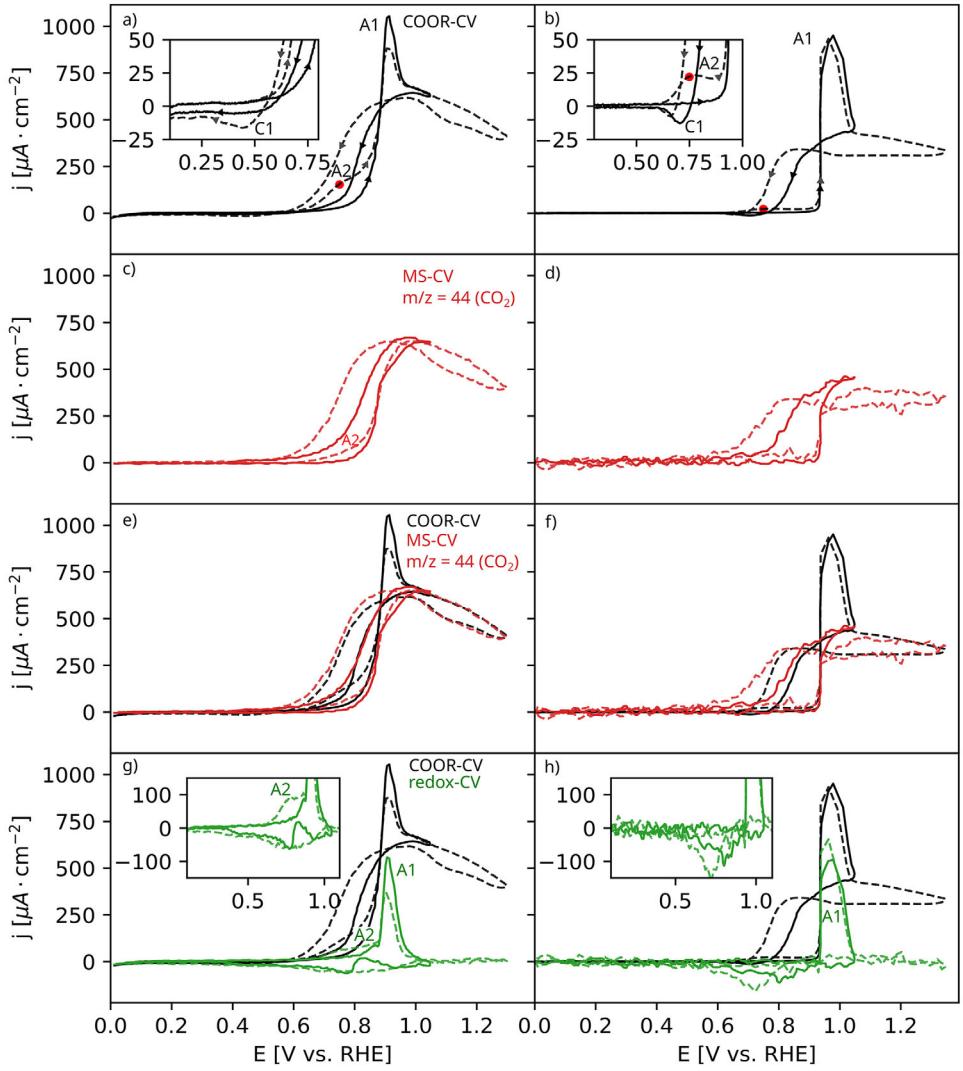

Figure 2. COOR on Pt-1 / Pt-3 electrodes (left / right column) recorded at 50 mV s^{-1} in CO saturated 0.5 M H_2SO_4. (a,b) Faraday current at the electrodes. The insets show the magnified region around the onset potential. (c,d) Mass spectrometry cyclic voltammograms obtained by normalizing the mass spectrometry signals for CO_2 formation (m/z=44) – MS-CVs in red. (e,f) Comparison of COOR-CVs with the MS-CVs. (g,h) Redox-CVs (in green), which are obtained by subtracting the MS-CVs from the COOR-CVs. The solid/dashed line shows the CVs with an UPL of 1.05 V/1.35 V. Arrows indicate the scan direction.

subtracting the MS-CV from the COOR-CV (black minus red curve in Figure 2e,f), yields a CV that represents other surface redox processes, as they are usually found in CVs recorded in CO-free electrolytes, plus contributions from CO_2 formation by reaction with preadsorbed OH/O species, which release less than the two electrons per CO_2 assumed in the calculation of the K-factor (see Section S3). We denote this curve as redox-CV, shown in green in Figure 2g,h (plotted along with the COOR-CV for comparison). Note that the curves represent sums of signals originating from regions with different Pt layer thicknesses, weighted by their contribution to the total surface area. Therefore, direct correlations between individual features in the signals and a specific film thickness are not possible. In the following, we describe the origin of the features and the resulting shape of the various CVs and MS-CVs, focusing on aspects relevant for the understanding of the restructuring processes found in the STM images above. Because of the broad Pt layer thickness distribution, a direct evaluation of layer-specific features and trends in activity is not possible from the present data. This must be addressed in a separate work.

Overall, the shape of the COOR-CVs is rather similar to those reported for Pt electrodes.[62,66–71] Based on these studies and previous ones on Pt-modified Ru(0001) electrodes, the processes taking place in different potential regions can be qualitatively described as follows. Starting with the positive-going scan from the low-potential limit up to the onset of the COOR (0.5 V for Pt-1 and 0.6 V for Pt-3), the surface is poisoned by CO, inhibiting any surface redox processes, as has been demonstrated for pure Pt[62,66–71] and Pt-modified Ru(0001) electrodes.[54,55,72–75] With the onset of OH/O formation on the surface (from water splitting) in the CO adlayer, the COOR starts, which had been described in detail for the COOR in CO-saturated electrolytes on pure Pt electrodes.[62,67,76] Note that the current density decreases slightly around the onset potential in the first potential cycles, which is

illustrated in Figure S3. A similar phenomenon has been reported for Pt(111) during the COOR in CO saturated 0.1 M $HClO_4$.[77] In this potential region, up to the onset of the reaction, the MS-CV closely follows the COOR-CV.

2.2.1. COOR with an UPL up to 1.05 V

From the COOR onset potential, the current density in the COOR-CV rises sharply, both for the Pt-1 and Pt-3 electrodes, resulting in a distinct peak **A1**. A similar behavior is commonly observed for bulk CO electro-oxidation on Pt electrodes.[62,66–70,78] Note that the MS-CV does not show a peak in the peak **A1** region, in contrast to earlier observations for the COOR on supported Pt/C catalyst electrodes and rough Pt ATR films.[70,79] The peak is also absent in further measurements on various Pt electrodes presented in Section S4. The additional peak **A1** in the CV must result from the rapid formation / uptake of OH/O species on the surface, which does not show up in the MS-CV signal.[78] This OH/O formation is apparent in a peak A1 in the positive going scan of the redox-CV in Figure 2g,h.

In the negative-going scan, the COOR shows a higher activity in the potential region around the onset potential of the COOR in the positive-going scan. Such a hysteresis is commonly observed for the COOR on Pt-modified Ru and also on pure Pt electrodes.[54,55,62,66–70,72–75,80] More important, the current density in the MS-CV seems to be slightly larger than that in the COOR-CV, which must be due to surface reduction processes taking place simultaneously in this potential region. This is discussed further in the next section. Once the current density decayed to zero in the COOR-CV, a reduction peak / region **C1** appears at more negative potentials, which is rather broad for Pt-1 and more peak-like for Pt-3 (see insets in Figure 2a,b and Figure S4). The appearance of this peak **C1** indicates that under present conditions, part of the surface OH/O adspecies are reduced to water instead of reacting with adsorbed CO. Nevertheless, the removal via the COOR is also possible, as indicated by a small current in the MS-CV in the potential region of peak **C1**. This also means that the observed current peak **C1** is a sum of currents related to the direct removal of OH/O from Pt to form water (negative current) and OH removed by the COOR (positive current). The total amount of removed, adsorbed OH/O, either by reduction to water or by reaction with CO, is presented in the redox-CVs in Figure 2g,h. These curves indicate the reductive or reactive OH/O removal in a peak / region for potentials below about 1.0 V for both electrodes. The oscillatory behavior of the reduction peak in the redox-CV is possibly an artefact caused by problems in the temporal correlation of the MS-CV and the COOR-CV.

2.2.2. COOR with an UPL up to 1.35 V

For the Pt-1 electrode, recording CVs with an UPL higher than 1.05 V leads to a shift of the onset potential for the COOR to lower potentials, apparent in a pre-peak or shoulder **A2** in the CV (Figure 2a and Figure S4). It appears for UPLs larger than 1.1 V. The assignment of this peak / shoulder **A2** to an earlier onset of the COOR is confirmed by an increase in the CO_2 current in the MS-CV in (Figure 2e). The extent of the current increase depends on the number of potential cycles at a given UPL and the applied UPL (see Figures S4 and S6). A similar phenomenon has been reported previously and has been attributed to a potential induced restructuring of the electrode surface,[53–55] which is also supported by the STM image in Figure 1e, recorded after the electrochemical measurements. It was suggested that newly formed low-coordinated sites on the restructured electrode enhance the COOR.[53–55] Apparently, continuing surface restructuring of the Pt-1 electrode reduces the formation of OH/O species on the Pt-1 surface in the peak **A1**, leading to a decrease in size of that peak. On the other hand, this restructuring also leads to an enhanced COOR activity in the region of peak **A2**. During restructuring, the newly formed sites with lower coordination will bind OH/O stronger than sites on the flat Pt layers, thus allowing OH/O formation on the surface already at lower potentials. Hence, this also leads to the peak **A2** in the redox-CV in Figure 2g (see inset), indicating OH/O adsorption in this potential region. Consequently, the restructuring reduces the number of sites on the flat Pt areas, leading to a decrease of Peak **A1** in the redox-CV. This is also evident for the Pt-2 electrode described in Section S5, where with an increasing number of potential cycles (with increasing UPL – Figure S6a or fixed UPL – Figure S6b), the COOR activity in the peak **A1** decreases even further. Finally, the current density decreases in the entire potential region where the Pt-2 electrode is active for the COOR. STM images recorded after the COOR for the fully restructured electrode indicate that the Pt film formed large agglomerates on the surface, exposing the severely restricted Ru(0001) surface.

For the Pt-3 electrode, such kind of restructuring induced increase of the COOR at around the onset potential is hardly visible in the COOR-CV upon extending the UPL up to 1.35 V (see inset of Figure 2b). The remaining subtle changes in the current density (one order of magnitude lower than for Pt-1) which are pronounced only at the onset of the reaction, with 20 μA cm^{-2} for Pt-3 and 150 μA cm^{-2} for Pt-1 at 0.75 V (see red dots in Figure Figure 2a), are tentatively associated with a slight restructuring of the electrode, possibly in the small fraction of mono- and bilayer Pt areas (see Figure 1d) present on the Pt-3 electrode, although this could not be resolved by STM imaging. The magnitude of peak **A1** remains almost unchanged during potential cycling for the Pt-3 electrode, different from the decrease for the Pt-1 electrode.

For potentials more positive than peak **A1**, the COOR current density declines with increasing potential, which is more pronounced for the Pt-1 than for the Pt-3 electrode. This potential region is often denoted as the mass transport-limited region.[70,81] In the present case, however, under enforced mass transport, kinetic limitations seem to be active as well, leading to the observed decay in COOR rate with increasing potential. The presence of kinetic limitations is also consistent with the lower COOR current on the Pt-3 electrode in this potential region as compared to the Pt-1 electrode (for similar flow rates). For each of the two electrodes, the current densities exhibit the same potential dependence for different UPLs. This is also true for the Pt-1 electrode, which tends to restructure under these conditions

(see Figure S4). Apparently, the processes responsible for the decay in COOR rate with increasing potential are fully reversible between subsequent cycles.

In the negative-going scan, the COOR current increases again in this potential region for the Pt-1 electrode, while for the Pt-3 electrode it remains about constant. The constant COOR current on the Pt-3 electrode indicates that the slight decline of the COOR rate due to the further accumulation of OH/O species on the surface in the positive-going scan, in addition to the amount formed in the peak **A1**, is not reversed, but also not continued. Thus, during the reaction, the coverage of these species remains constant in this potential range. Their amount can only be reduced at lower potential. In this case, the kinetic limitations remain present in the negative-going scan in this potential range. This also means that the difference in COOR rates between the positive-going and the negative-going scan increases with increasing UPL. For the Pt-1 electrode, the reasons for the pronounced decay in COOR rate at potentials positive of peak **A1** are largely, though not completely, removed in this potential range, leading to only small differences in the COOR current between the positive-going and negative-going scans at the potential directly above the peak **A1**. Furthermore, different from the Pt-3 electrode, this removal of the kinetic limitations always leads to the same current at about 0.95 V, independent of the UPL. Therefore, for this electrode, most of the more pronounced COOR current decay in the positive-going scan in this potential range must be due to reversible processes such as reversible accumulation and replenishment of additional adsorbed OH/O species or the reversible buckling of Pt surface atoms due to insertion of oxygen atoms underneath, which was described as reversible extraction during the oxidation of Pt(111).[82,83] Only a small part of this decay in activity is caused by processes that cannot be reversed in this potential range.

In the potential range of the peak **A1** and below in the negative-going scan, increasing the UPL results in a shift of the steep decline in COOR current to lower potentials, both for the Pt-1 and the Pt-3 electrode. Since the steep increase of the COOR current in the positive-going scan does not shift significantly, the hysteresis becomes broader with increasing UPLs. Starting with the Pt-3 electrode, the shift of the steeply declining COOR current to lower potentials with increasing UPL must be due to an increasing amount of OH/O species on the surface, which lowers the COOR rate at potentials positive of 1.0 V. These species can support the COOR for a longer time and thus to lower potential in the scan. Once most of these species are consumed reactively, rapid blocking of the surface by adsorbed CO sets in. This explanation closely agrees with previous modeling results for CO bulk oxidation on Pt, where such shifts had been related to the larger degree of OH/O formation on the sample at high potentials.[80]

For the Pt-1 electrode, where the COOR current in the potential range of the peak **A1** does not seem to vary with the UPL, the explanation must be more complex. Clearly, one would expect a similar physical reason for the observed down-shift in the COOR current decline for potentials more negative than peak **A1** as for the Pt-3 electrode. However, in the case of the Pt-1 electrode, restructuring effects must also be considered, which may further affect the COOR rate at potentials lower than peak **A1**.

Once the COOR rate has decreased to zero, we now observe a distinct reduction peak **C1** in the COOR-CVs (instead of a reduction region observed for lower UPLs, see above), which must be related to the electrochemical removal of OH/O species or metal oxides formed at high overpotentials by reduction. This peak increases with increasing UPL for the Pt-1 electrode, while for the Pt-3 electrode, it seems to decrease (see insets and Figure S4). For the Pt-3 electrode, we suggest that this apparent decrease of the peak **C1** (and shift to lower potential) is caused by an increasing overlap between the steeply declining COOR current and the peak **C1** reduction peak. For the Pt-1 electrode, the reduction peak is located at more negative potentials than the declining COOR curves. Here, the increase in peak **C1** can be rationalized by increasing amounts of OH/O species formed on the exposed Ru(0001) substrate.[53,54,84] In the redox-CV in Figure 2g,h, the reduction peak for OH/O removal (see inset) has a similar size for both electrodes and seems to be mostly independent from the applied UPL. The shape varies slightly, and the peak maximum is at slightly different potentials. In principle, if our suggestion from above is correct, that the amount of OH increases at higher UPLs, then the charge within that peak should increase. Such information can, however, not be confirmed from the present data.

2.3. MOR – SXRD

Next, we present the results of combined CV and SXRD measurements performed on a Pt-3 electrode in pure and 0.1 M MeOH containing 0.5 M H_2SO_4. In this case, the potential was cycled between 0.05 and 1.4 V, while the surface sensitive (1 0 2.35) reflection was monitored (Figure 3). The Experimental Section and Section S6 contain further information about the synchrotron measurements. Note that the SXRD intensity curves also represent sums of signals originating from regions with different Pt layer thicknesses or adsorbed species, weighted by their contribution to the total surface area. Therefore, direct correlations between individual features in the signals and a specific Pt film thickness are not possible. For the sake of completeness, additional CVs and SXRD curves illustrating the effect of changing the UPLs from 1.05 to 1.40 V are shown in Section S6, including also information on the noise in the CV data. CVs recorded in 0.5 M H_2SO_4 on similar electrodes in the DEMS set-up are shown in Figures S1 and S2.

Despite the considerable noise, the CV (blue curve in Figure 3a) resolves a slight increase in the current density in the positive-going scan above 0.8 V, which coincides with the onset of a steep decrease in the X-ray intensity. Previously, we had attributed a current increase (or peak) in this potential region to the desorption of bisulfate and the simultaneous adsorption of OH.[52] Note that a possible exchange of bisulfate with OH in a 1:1 ratio would not show up in the CV since the net current density will be zero.[85] Therefore, the actual onset for surface OH formation cannot be deduced directly from the CV and might even occur at lower potentials than the onset of the surface OH/O formation current. In general, the adsorption of OH/O will lead to a change in the interlayer spacing of the topmost Pt

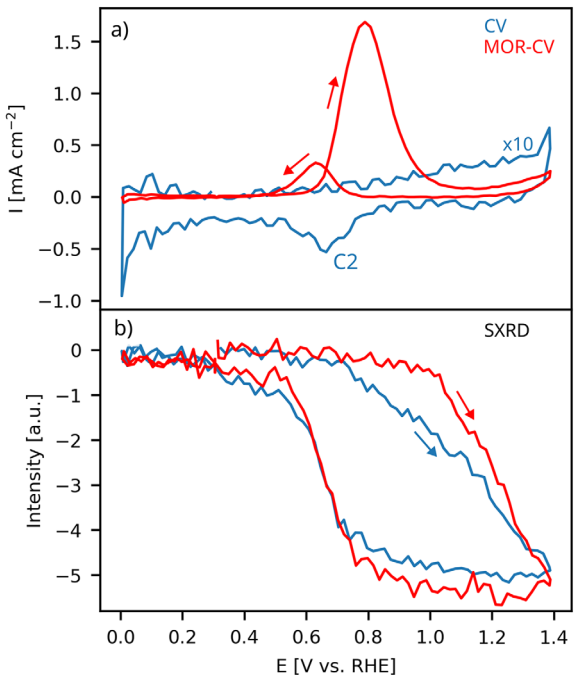

Figure 3. (a) Comparison of CVs recorded on a Pt-3 electrode in 0.5 M H_2SO_4 (blue, upscaled by a factor of 10) and in 0.2 M MeOH in 0.5 M H_2SO_4 (red) - MOR. The CVs were recorded at 20 mV s^{-1}. (b) Evolution of the SXRD intensity at the (1 0 2.35) reflection recorded along with the CVs in (a).

atoms, which is reflected in a change in the X-ray intensity. In recent SXRD studies on the electro-oxidation of single-crystal Pt surfaces, a pronounced reversible decrease (positive-going scan) and increase (negative-going scan) of the SXRD intensity in the (0 1 1.5)[83] and (1 1 1.5)[82] reflections was attributed to a reversible buckling of the Pt surface, involving a partial extraction of Pt surface atoms by reversible incorporation and removal of subsurface oxygen. On Pt(111), the onset for this process is at about 1.1 V.[82] Earlier onsets for this process were reported for Pt(100) surfaces or carbon-supported Pt particles.[57,86] Considering also the significant change in XRD intensity, we assume that the decrease observed here is primarily related to the reversible extraction of part of the Pt atoms. From the present data, we cannot distinguish whether this extraction occurs on the terraces or predominantly on defect sites (step edges and regions on the electrode that might not be as perfectly structured as those presented in the STM images in Figure 1d). Changes in X-ray intensity due to desorption of bisulfate and adsorption of OH/O on the terrace sites are expected to be much smaller (see below). In the reverse, negative-going scan, the X-ray intensity starts to increase steeply at around 0.8 V, coinciding with the onset of a small reduction peak **C2** in the CV. We associate this increase with the reversible removal of O atoms from subsurface sites and the de-buckling of the related Pt surface atoms, accompanied by reductive OH/O desorption and possibly bisulfate adsorption, which, however, does not fully compensate for the OH/O removal charge. After a complete potential cycle, the X-ray intensity reaches its original value. Further CVs recorded with increasing UPLs do not change significantly, suggesting that the surface did not irreversibly restructure substantially. Subtle changes in the CVs recorded for different UPLs, both in the combined SXRD-CV measurements as well as in CVs recorded in a dedicated electrochemical setup, are described and discussed in the SI.

MOR measurements performed on these electrodes after the cyclic voltammetry measurements in the supporting electrolyte (red curves in Figure 3) resemble those recorded in the MOR on Pt electrodes.[87–89] Adsorbed CO blocks the surface at low potentials, resulting in a negligible reaction current. The current starts to increase in the positive-going scan at around 0.6 V. Interestingly, although a detailed picture of the product composition is still missing, the formation of CO_2 close to the onset potential of the MOR is negligible.[52] Hence, in this potential range, formaldehyde or formate / formic acid are the most likely products formed on Pt-3. After passing through a maximum at about 0.8 V, the current density decreases again and reaches negligible values at around 1.1 V. Formerly, it was suggested that this current density decrease is associated with OH/O adlayer formation on the surface, with adsorbed OH/O blocking the surface for the MOR.[87–89] Also, in the negative-going scan, the electrode becomes only active for the MOR once the OH/O adlayer starts to be reductively removed at around 0.8 V (see below).

The evolution of the X-ray intensity at the (1 0 2.35) position during the MOR (red curve) is very similar to that obtained in the pure supporting electrolyte, except that the onset of the sharp decrease in the positive-going scan shifts by 300 mV to more positive potentials, from 0.8 to 1.1 V. As mentioned above, the reversible insertion of adsorbed O atoms together with the partial extraction of the associated Pt surface atoms was suggested to be the dominant process in this potential region in the pure supporting electrolyte, which accounts for this change. Still, there is a slow decay in X-ray intensity in the potential range between the MOR peak maximum at about 0.8 V and the end of this peak at about 1.1 V, which is possibly related to the adsorption of OH/O on the surface, inhibiting the MOR. The up-shift to 1.1 V of the steep decrease of the X-ray intensity indicates that the associated process is mostly inhibited in this potential range during the MOR, as compared to measurements in the pure supporting electrolyte on Pt-3. Most likely, this up-shift is caused by a reaction of OH/O (possibly at defect sites as described above) with methanol or with reaction intermediates formed during the MOR, which lowers the steady-state OH/O coverage at a given potential and thus shifts the coverage-potential curve to higher potential, in agreement with the up-shift of the onset of the steep decline of the X-ray intensity observed experimentally. Surface-enhanced infrared reflective adsorption spectroscopy (SEIRAS) measurements on pure polycrystalline Pt electrodes indicated that the adsorbed CO blocking the surface before the MOR onset is entirely removed at the MOR peak maximum.[90,91] Hence, also adsorbed CO could block the OH/O adsorption and consequently also O insertion / Pt extraction in the potential range up to the X-ray intensity decrease. Furthermore, with the onset of the MOR, adsorbed formate ($HCOO_{ad}$) was found to form on the surface, with the SEIRAS intensity following the MOR current density in both scan direc-

tions, which can contribute to the slow decay in X-ray intensity in this potential region.

Finally, based on the reversibility of the X-ray intensity, we can rule out that the decline in X-ray intensity at higher potentials is related to any irreversible surface restructuring. This is also supported by additional STM measurements performed after the *operando* SXRD measurements under UHV conditions, which indicated that the Pt-3 electrodes are indeed very stable under present MOR reaction conditions (see Section S6).

2.4. Discussion

The results presented above for the Pt-1 and Pt-3 electrodes, as well as those for Pt-2 (Section S5), have shown that in the COOR during potential cycles up to 1.35 V, the monolayer Pt film is more stable against irreversible restructuring than bilayer islands on the monolayer film and that three to four-layer films remain almost unchanged. Bilayer Pt films also seem to be less stable in CO-free electrolytes, as shown in Figure S1. For the Pt-3 electrode, a high stability was also shown for the MOR up to 1.4 V. In the following, we briefly discuss possible reasons for these differences in the layer-dependent stability and draw comparisons with Pt(111).

Traditionally, surface restructuring of Pt(111) electrodes during oxidation and reduction cycles in pure acidic electrolytes (with an UPL larger than 1.2 V) was rationalized by an irreversible place exchange process between adsorbed atomic oxygen and surface Pt atoms.[56–60] More recently, this picture was supplemented by a reversible O insertion / partial Pt extraction process, which occurs before irreversible Pt and O exchange. In a simple picture, one would expect that both reversible and irreversible restructuring of the Pt surface layer(s) set in once a critical coverage of adsorbed OH/O species is reached.[57] For Pt layers on Ru(0001), it is known that the binding energy of OH/O is lowest on the monolayer and increases with increasing Pt layer thickness, until reaching the binding energy of Pt(111) for thick layers.[40] In that case, the onset of restructuring should shift to lower potentials with increasing Pt layer thickness, and the critical potential for the onset of a possible irreversible place exchange process would then always be more positive than that for Pt(111), which is around 1.2 V. Hence, the Pt films on Ru(0001) should, in principle, be intrinsically more stable than Pt(111) with respect to reversible Pt extraction and irreversible place exchange, with monolayer Pt films presenting the most stable structure. Since the Pt-3 electrodes are stable under present reaction conditions, the potential for irreversible place exchange processes must be beyond the explored potential limit of 1.35 V for the COOR or 1.4 V for the MOR. Furthermore, considering that both irreversible place exchange and dissolution lead to a restructuring of the surface, this also means that the Pt dissolution potential should shift to more positive potentials. On the other hand, once the critical potential for the formation of a dense O adlayer is reached, we expect that the Pt films on Ru(0001) restructure similarly to Pt(111) electrodes along with Pt dissolution. Indeed, we found similar structures as for restructured Pt(111) on Pt-3 electrodes, induced by potential cycles to high potentials in the pure supporting electrolyte shown (in Section S1).

In contrast to the above argumentation, however, we observed that very thin Pt films (incomplete Pt monolayer or bilayer films) are less stable than Pt(111). We suggest that the enhanced restructuring tendency of the (incomplete) monolayer film is induced by the strong interaction of OH/O species with the Ru(0001) substrate, which must be considered. Apparently, the gain in energy provided by the strong interaction of OH/O species with Ru(0001) is sufficient to displace Pt from monolayer sites into next layer sites, providing space for an additional uptake of OH/O species on the Ru(0001) substrate. Computational works showed that Pt atoms in the second layer bind less strongly on the first Pt layer than Pt atoms directly attached to the Ru(0001) substrate.[40] However, this loss in energy is apparently overcompensated by the energy gain of the OH/O adspecies, if they are strongly adsorbed on Ru(0001) rather than weakly adsorbed on a Pt monolayer film. The energy gain of the entire system upon OH/O-induced displacement of Pt atoms into the second or higher layers provides the energetic driving force for such kind of restructuring. For the Pt-2 electrode, the COOR data indicate that these electrodes seem relatively stable when the layer is closed (up to 1.3 V, see Section S5 in the SI), which does not seem to be the case in the CO-free supporting electrolyte (Section S4 in the SI). Based on the explanations above, we would expect that Pt bilayers are less stable than the monolayer but also more stable than the trilayer films. The physical origin of this discrepancy is so far open.

During the MOR, we observed a shift of the decrease in X-ray intensity to more positive potentials compared to the measurements in the MeOH-free electrolyte. This effect was rationalized by a potential dependent lowering of the OH/O adsorbate coverage and thus by a similar up-shift of the O insertion and Pt extraction in the presence of methanol or reaction intermediates formed during the MOR. We suggest that a similar shift of the decrease in X-ray intensity to more positive potentials, as observed in the SXRD measurements in the MOR, will occur also during the COOR. In that case, the effect might be even more pronounced since CO oxidation also occurs up to the OER. CO can readily adsorb and react on the electrode surface, even by chemical reaction with Pt surface oxides. In contrast, active intermediates can only be formed in the MOR by splitting MeOH, which is increasingly hindered at high potentials. Therefore, we assume that CO in the CO-saturated solution can efficiently remove OH/O species from the surface even at a potential where the MOR is inhibited, and thus shift the potential for partial Pt extraction and reversible surface restructuring to even more positive potentials. Accordingly, also the potential for irreversible restructuring may be up-shifted.

Finally, we address the relevance of our results for realistic Ru-core Pt-shell particles that have been used as highly efficient catalysts in various reactions, as presented in the introduction. Although our measurements on planar electrodes do not allow conclusions on facet-specific differences in stability that can be present on more complex supported particles, they nevertheless

demonstrate that the main requirement for Pt-core Ru-shell catalysts is that Pt must completely cover the entire Ru substrate to prevent Ru dissolution or Pt restructuring induced by the strong interaction of OH/O species with Ru. We assume that this aspect is also true for other Ru surface orientations. For closed Pt layers and reactions such as the ORR, HER, and HOR, a possible restructuring by an irreversible place exchange process is presumably negligible, since these reactions normally proceed at potentials well below the onset potential of restructuring, which for these systems is higher than that for pure Pt. In the presence of oxidizable species in the feed, one could expect even a higher stability since their reaction with OH/O species would decrease the steady-state coverage of these latter species at a given potential and thus shift the onset potential for surface restructuring to higher potentials. The detailed understanding of the layer-dependent stability of such systems is, however, still incomplete. Earlier studies indicated that Ru-core Pt-shell systems with two layers of Pt are rather stable,[14,37] which is not the case for well-defined Pt layers on Ru(0001). These discrepancies are most likely due to the different structural properties, e.g., different surface orientations on the core-shell particles compared to the present model systems.

3. Conclusion

Using Ru(0001) electrodes covered by a monolayer and three layers of Pt, we demonstrate by DEMS measurements during the COOR and by *operando* SXRD measurements during the MOR, as well as by STM imaging before and after the electrocatalytic investigation, that submonolayer Pt films start to restructure for potentials more positive than 1.1 V (as shown previously), in contrast to films with three layers (and more), which are stable up to about 1.4 V during the COOR and MOR.

1. We suggest that the (sub)monolayer films are less stable due to the strong adsorption of OH/O species on bare Ru(0001), which provides sufficient driving force for restructuring the Pt film areas.
2. The higher stability of three-layer Pt films toward restructuring during the MOR and COOR in acid electrolyte, also in comparison to bare Pt(111) electrodes, suggests that the potential for reversible surface restructuring shifts to more positive potentials. This shift is attributed to a weaker bonding of OH/O species on the three-layer Pt film than for the adsorption on Pt(111).
3. From the SXRD measurements, we conclude that, in general, the electro-oxidation of organic molecules reactively reduces the potential dependent steady-state coverage of surface OH/O species, which needs to reach a critical value before it can induce structural changes. This increases the stability range of the respective Pt electrode, as compared to the situation in the pure supporting electrolyte.

Overall, this work demonstrates the high potential of model studies on complex but structurally well-defined electrodes, employing various *operando* techniques for providing a qualitative atomic scale understanding of the stability of complex electrocatalyst systems during the oxidation of organic molecules.

4. Experimental Details

The Pt-modified Ru(0001) single-crystal electrodes used in this work were prepared and characterized by STM under UHV conditions at the Institute of Surface Chemistry and Catalysis at Ulm University (Ulm, Germany). The electrochemical DEMS characterization was performed in Ulm and the combined electrochemical and SXRD measurements at the ID03 beamline of the European Synchrotron Radiation Facility (ESRF, Grenoble, France). Where necessary, we indicate facility-specific experimental details.

4.1. Materials

The acid solutions were prepared from high-grade chemicals and MilliQ water (18.2MΩ cm). For the measurements performed in Ulm, we used H_2SO_4 Merck Suprapure 98% and methanol Merck EMSURE®. The electrolytes were purged with N_2 (Westfalen 6.0). For the measurements performed at the ESRF, the solutions were prepared from H_2SO_4 93% –98%, VWR ARISTAR®ULTRA and methanol (Fluka Analytical, LC-MS Ultra Chromasolv®). The electrolytes were purged with Ar (Air Liquide, BIP grade).

The Ru(0001) single crystal electrodes were purchased from MaTecK GmbH (purity 99.99%, orientation accuracy $<0.1°$). The hat-shaped (2 mm thickness, 10 mm front diameter / 12 mm back side diameter) single crystal electrodes are mounted in a Ta sample holder.

The glassware was cleaned before each experiment by storage in highly concentrated KOH (Ulm) or Piranha etch (ESRF) overnight. Subsequently, it was thoroughly boiled and rinsed with hot MilliQ water.

4.2. Sample Preparation

The Ru(0001) electrodes were prepared under UHV conditions in an experimental set-up described elsewhere.[92] Clean and atomically flat surfaces were obtained by several cycles of Ar ion sputtering ($p_{Ar} = 3 \times 10^{-5}$ mbar, $I = 4\,\mu A\,cm^{-2}$, t = 30 min) and flash annealing to 1600 K, followed by seven cycles of flash annealing to 1600 K and adsorption of 10 L of O_2 at $T < 600$ K during sample cooling to remove carbon impurities, finished by three flash annealing cycles to 1600 K without O_2 adsorption. Pt was deposited by means of electron beam physical vapor deposition with an Omicron EFM-3 evaporator at a rate of ca. 0.1 ML min^{-1}. During the deposition process, the sample was held at 670 K to improve the Pt layer-by-layer growth.[41,49,52,55] Higher deposition temperatures must be avoided to prevent surface alloy formation.[48,93]

4.3. Structural Characterization from STM Imaging

The quality of the freshly prepared Ru(0001) samples, the amount of Pt deposited, and the structural properties of the Pt films were investigated with STM under UHV conditions. The deposi-

Table 1. Platinum layer thickness distribution including areas exposed by Ru(0001), given in %, for samples with different Pt coverage Θ_{Pt}.

		Pt layer				
Θ_{Pt}	Ru	1	2	3	4	5
1.0 ML	1.5	66	32.5	0	0	0
2.2 ML	0	14.5	58	22.5	4.5	0
3.5 ML	0	0.05	3	44	51.5	1.5

tion rate was frequently determined from STM images recorded on electrodes with submonolayers of Pt, prepared by depositing Pt on a freshly prepared Ru(0001) electrode either before the Pt multilayer growth (long evaporation times) or afterward on a second R(0001) sample. To validate the homogeneity of the evaporation process on the entire sample surface, STM images were usually recorded in macroscopically different spots on the electrode (separated by several mm). The Pt layer thickness distribution, inferred from the STM images, for Pt coverages used in this work, is shown in Table 1. The distributions are in line with those reported previously.[52]

4.4. Electrochemical Characterization

In Ulm, the electrochemical characterization of the Pt-modified Ru(0001) electrodes was performed in a dual thin-layer flow cell in a DEMS configuration, which is described elsewhere.[65] Before the experiments, the flow cell, including all inlet capillaries, was thoroughly rinsed with hot MilliQ water. For this work, we used a home-built RHE as a reference electrode (RE) and a Au wire as a counter electrode (CE). The potential was controlled with a Pine AFRDE5 bi-potentiostat, and the data were acquired with an in-house programmed software. The different measurement procedures are described in Section S2. A detailed description of the calibration of the DEMS signals is provided in Section S3.

At the ESRF, the electrochemical measurements were performed in an electrochemical cell that allows for *operando* SXRD measurements, which is similar to the one described in Ref. [94]. For this work, we employed a Ag|AgCl|3.5M KCl (eDaq company) RE and a glassy carbon CE. The potential was controlled with a Biologic SP300 potentiostat. All potentials were converted to the RHE scale. A more detailed description of the electrochemical procedure at the ESRF is provided in the Section. S6.

4.5. SXRD

The X-ray measurements were performed at the ID03 beamline of ESRF in Grenoble. The 24 keV X-ray beam was focused to a size of 300 μm × 50 μm (horizontal × vertical relative to the plane of the sample surface) at the sample position. The incidence angle of the beam was set to 0.3° relative to the surface plane. The data were collected with a 2D Maxipix detector and analyzed as described in Ref. [95]. The relative reciprocal space units used for the reflection indexing are determined from the Ru(0001) surface unit cell with the following parameters (*c* perpendicular to the surface plane): $a = 2.7059$ Å, $b = 2.7059$ Å, $c = 4.2815$ Å, $\alpha = 90°$, $\beta = 90°$, and $\gamma = 120°$.

Acknowledgements

The authors would also like to thank Helena Isern and Thomas Dufrane for technical support at ID03 beamline at ESRF. The work in Ulm contributes to the research performed at CELEST (Center for Electrochemical Energy Storage Ulm-Karlsruhe). The authors thank Jens Klein (formerly Ulm University) for providing additional data for the SI.

Open access funding enabled and organized by Projekt DEAL.

Conflict of Interests

The authors declare no conflict of interest.

Author Contributions

Albert K. Engstfeld: Conceptualization; software; visualization; supervision; investigation; formal analysis; writing—original draft preparation; data curation. **Lukas Forschner**: Investigation; writing—reviewing and editing. **Mario Löw**: Investigation. **Linus Pithan**: Investigation; supervision. **Paul Beyer**: Investigation; supervision. **Zenonas Jusys**: Investigation; writing—reviewing and editing. **Joachim Bansmann**: Investigation; writing—reviewing and editing. **R. Jürgen Behm**: Writing —reviewing and editing; resources; funding acquisition. **Jakub Drnec**: Writing—reviewing and editing; resources; funding acquisition; data curation, investigation; formal analysis; software.

Data Availability Statement

The data that support the findings of this study are openly available in Zenodo at https://doi.org/10.5281/zenodo.14083383, reference number 14083383.

Keywords: Core-shell particles · Electrocatalysis · Electrode stability · Model electrodes · SXRD

References

[1] X. Zhao, K. Sasaki, *Acc. Chem. Res.* **2022**, *55*, 1226–1236.
[2] J. Sachtler, J. Biberian, G. Somorjai, *Surf. Sci.* **1981**, *110*, 43–55.
[3] M. B. Gawande, A. Goswami, T. Asefa, H. Guo, A. V. Biradar, D.-L. Peng, R. Zboril, R. S. Varma, *Chem. Soc. Rev.* **2015**, *44*, 7540–7590.
[4] S. Das, J. Pérez-Ramírez, J. Gong, N. Dewangan, K. Hidajat, B. C. Gates, S. Kawi, *Chem. Soc. Rev.* **2020**, *49*, 2937–3004.
[5] J. R. Kitchin, J. K. Nørskov, M. A. Barteau, J. Chen, *Phys. Rev. Lett.* **2004**, *93*, 156801.
[6] R. R. Adzic, J. Zhang, K. Sasaki, M. B. Vukmirovic, M. Shao, J. Wang, A. U. Nilekar, M. Mavrikakis, J. Valerio, F. Uribe, *Top. Catal.* **2007**, *46*, 249–262.
[7] M. Mavrikakis, B. Hammer, J. K. Nørskov, *Phys. Rev. Lett.* **1998**, *81*, 2819.

[8] Calle- F. Vallejo, M. T. Koper, A. S. Bandarenka, *Chem. Soc. Rev.* **2013**, *42*, 5210–5230.
[9] L. Yang, M. B. Vukmirovic, D. Su, K. Sasaki, J. A. Herron, M. Mavrikakis, S. Liao, R. R. Adzic, *J. Phys. Chem. C* **2013**, *117*, 1748–1753.
[10] D. Takimoto, T. Ohnishi, J. Nutariya, Z. Shen, Y. Ayato, D. Mochizuki, A. Demortière, A. Boulineau, W. Sugimoto, *J. Catal.* **2017**, *345*, 207–215.
[11] J. Svendby, F. Seland, G. Singh, J. L. G. de la Fuente, S. Sunde, *J. Electroanal. Chem.* **2019**, *833*, 189–197.
[12] A. Jackson, V. Viswanathan, A. J. Forman, A. H. Larsen, J. K. Nørskov, T. F. Jaramillo, *ChemElectroChem* **2014**, *1*, 67–71.
[13] A. Jackson, A. Strickler, D. Higgins, T. F. Jaramillo, *Nanomaterials* **2018**, *8*, 38.
[14] Y.-C. Hsieh, Y. Zhang, D. Su, V. Volkov, R. Si, L. Wu, Y. Zhu, W. An, P. Liu, P. He, S. Ye, R. R. Adzic, J. X. Wang, *Nat. Commun.* **2013**, *4*, 2466.
[15] S. Alayoglu, A. U. Nilekar, M. Mavrikakis, B. Eichhorn, *Nat. Mater.* **2008**, *7*, 333–338.
[16] S. Alayoglu, P. Zavalij, B. Eichhorn, Q. Wang, A. I. Frenkel, P. Chupas, *Acs Nano* **2009**, *3*, 3127–3137.
[17] K. Elbert, J. Hu, Z. Ma, Y. Zhang, G. Chen, W. An, P. Liu, H. S. Isaacs, R. R. Adzic, J. X. Wang, *ACS Catal.* **2015**, *5*, 6764–6772.
[18] J. X. Wang, Y. Zhang, C. B. Capuano, K. E. Ayers, *Sci. Rep.* **2015**, *5*, 12220.
[19] E. N. El Sawy, P. G. Pickup, *Electrocatalysis* **2016**, *7*, 477–485.
[20] A. Hoang, E. El Sawy, A. Blackburn, S. Ketabi, M. Goledzinowski, F. J. Comeau, V. Birss, *ACS Appl. Energy Mater.* **2020**, *3*, 8423–8436.
[21] J. Zou, M. Wu, S. Ning, L. Huang, X. Kang, S. Chen, *ACS Sustainable Chem. Eng.* **2019**, *7*, 9007–9016.
[22] F. H. B. Lima, E. R. Gonzalez, *Appl. Catal., B* **2008**, *79*, 341–346.
[23] A. H. Ali, P. G. Pickup, *ECS Adv.* **2023**, *2*, 024501.
[24] M. Tsypkin, J. L. G. de la Fuente, S. G. Rodríguez, Y. Yu, P. Ochal, F. Seland, O. Safonova, N. Muthuswamy, M. Rønning, D. Chen, others, *J. Electroanal. Chem.* **2013**, *704*, 57–66.
[25] T.-Y. Chen, T.-L. Lin, T.-J. M. Luo, Y. Choi, J.-F. Lee, *ChemPhysChem* **2010**, *11*, 2383–2392.
[26] E. N. El Sawy, H. A. El-Sayed, V. I. Birss, *Phys. Chem. Chem. Phys.* **2015**, *17*, 27509–27519.
[27] N. Muthuswamy, J. L. G. de la Fuente, D. T. Tran, J. Walmsley, M. Tsypkin, S. Raaen, S. Sunde, M. Rønning, D. Chen, *Int. J. Hydrogen Energy* **2013**, *38*, 16631–16641.
[28] J. Xie, Q. Zhang, L. Gu, S. Xu, P. Wang, J. Liu, Y. Ding, Y. F. Yao, C. Nan, M. Zhao, others, *Nano Energy* **2016**, *21*, 247–257.
[29] D. Bokach, J. G. de la Fuente, M. Tsypkin, P. Ochal, Endsjø, I., R. Tunold, S. Sunde, F. Seland, *Fuel Cells* **2011**, *11*, 735–744.
[30] E. Antolini, *J. Solid State Electrochem.* **2011**, *15*, 455–472.
[31] O. Vinogradova, D. Krishnamurthy, V. Pande, V. Viswanathan, *Langmuir* **2018**, *34*, 12259–12269.
[32] M. Pourbaix, *NACE* **1966**, http://sunlight.caltech.edu/aic/pourbaix.pdf
[33] N. Hodnik, Jovanovič, P., Pavlišič, A., Jozinovič, B., M. Zorko, M. Bele, V. S. Šelih, M. Šala, S. Hočevar, M. Gaberšček, *J. Phys. Chem. C* **2015**, *119*, 10140–10147.
[34] O. A. Petrii, *J. Solid State Electrochem.* **2008**, *12*, 609.
[35] Y. V. Tolmachev, O. Petrii, *J. Solid State Electrochem.* **2017**, *21*, 613–639.
[36] V. Berova, A. G. Manjón, M. V. Paredes, T. Schwarz, N. A. Rivas, K. Hengge, T. Jurzinsky, C. Scheu, *J. Power Sources* **2023**, *554*, 232327.
[37] A. G. Manjón, M. Vega-Paredes, V. Berova, T. Gänsler, T. Schwarz, Rivas, N. A. R., K. Hengge, T. Jurzinsky, C. Scheu, *Nanoscale* **2022**, *14*, 18060–18069.
[38] J. Erlebacher, D. Margetis, *Phys. Rev. Lett.* **2014**, *112*, 155505.
[39] A. Schlapka, M. Lischka, A. Groß, U. Käsberger, P. Jakob, *Phys. Rev. Lett.* **2003**, *91*, 016101.
[40] M. Lischka, C. Mosch, A. Groß, *Electrochim. Acta* **2007**, *52*, 2219–2228.
[41] H. E. Hoster, O. B. Alves, M. T. Koper, *ChemPhysChem* **2010**, *11*, 1518–1524.
[42] F. B. de Mongeot, M. Scherer, B. Gleich, E. Kopatzki, R. Behm, *Surf. Sci.* **1998**, *411*, 249–262.
[43] A. Groß, *Top. Catal.* **2006**, *37*, 29–39.
[44] H. Hartmann, T. Diemant, J. Bansmann, R. J. Behm, *Phys. Chem. Chem. Phys.* **2012**, *14*, 10919–10934.
[45] P. Gazdzicki, P. Jakob, *Phys. Chem. Chem. Phys.* **2013**, *15*, 1460–1470.
[46] P. Gazdzicki, S. Thussing, P. Jakob, *J. Phys. Chem. C* **2011**, *115*, 23013–23022.
[47] P. Jakob, A. Schlapka, *Surf. Sci.* **2007**, *601*, 3556–3568.
[48] T. Diemant, A. Bergbreiter, J. Bansmann, H. E. Hoster, R. J. Behm, *ChemPhysChem* **2010**, *11*, 3123–3132.
[49] M. Schilling, S. Brimaud, R. J. Behm, *Phys. Chem. Chem. Phys.* **2017**, *19*, 22434–22443.
[50] M. Schilling, S. Brimaud, R. J. Behm, *Surf. Sci.* **2018**, *676*, 30–38.
[51] S. Brimaud, A. Engstfeld, O. Alves, H. Hoster, R. J. Behm, *Top. Catal.* **2014**, *57*, 222–235.
[52] J. Klein, F. Argast, A. K. Engstfeld, S. Brimaud, R. J. Behm, *Electrochim. Acta* **2019**, *311*, 244–254.
[53] A. K. Engstfeld, S. Brimaud, R. J. Behm, *Angew. Chem., Int. Ed.* **2014**, *53*, 12936–12940.
[54] A. K. Engstfeld, J. Klein, S. Brimaud, R. J. Behm, *Surf. Sci.* **2015**, *631*, 248–257.
[55] A. K. Engstfeld, J. Klein, S. Brimaud, *ChemPhysChem* **2021**, *22*, 828–832.
[56] M. Ruge, J. Drnec, B. Rahn, F. Reikowski, D. A. Harrington, F. Carlà, R. Felici, J. Stettner, O. M. Magnussen, *J. Am. Chem. Soc.* **2017**, *139*, 4532–4539.
[57] T. Fuchs, J. Drnec, F. Calle-Vallejo, N. Stubb, D. J. Sandbeck, M. Ruge, S. Cherevko, D. A. Harrington, O. M. Magnussen, *Nat. Catal.* **2020**, *3*, 754–761.
[58] T. Fuchs, V. Briega-Martos, J. Drnec, N. Stubb, I. Martens, F. Calle-Vallejo, D. A. Harrington, S. Cherevko, O. M. Magnussen, *Angew. Chem., Int. Ed.* **2023**, e202304293.
[59] L. Jacobse, Y.-F. Huang, M. T. Koper, M. J. Rost, *Nat. Mater.* **2018**, *17*, 277–282.
[60] K. Itaya, S. Sugawara, K. Sashikata, N. Furuya, *J. Vac. Sci. Technol. A: Vac. Surf. Films* **1990**, *8*, 515–519.
[61] J. Klein, S. Brimaud, A. K. Engstfeld, R. J. Behm, *Electrochim. Acta* **2019**, *306*, 516–528.
[62] J. Klein, V. Chesnyak, M. Löw, M. Schilling, A. K. Engstfeld, R. J. Behm, *J. Am. Chem. Soc.* **2019**, *142*, 1278–1286.
[63] Z. Jusys, R. Behm, *Encyclopedia of Electrochemical Power Sources*, 2nd Edition, Vol. *2*, Elsevier, Amsterdam, **2025**, pp. 77–104.
[64] P. P. Lopes, D. Tripkovic, P. F. Martins, D. Strmcnik, E. A. Ticianelli, V. R. Stamenkovic, N. M. Markovic, *J. Electroanal. Chem.* **2018**, *819*, 123–129.
[65] J. Schnaidt, S. Beckord, A. K. Engstfeld, J. Klein, S. Brimaud, R. J. Behm, *Phys. Chem. Chem. Phys.* **2017**, *19*, 4166–4178.
[66] C. A. Angelucci, F. C. Nart, E. Herrero, J. M. Feliu, *Electrochem. Commun.* **2007**, *9*, 1113–1119.
[67] C. A. Angelucci, E. Herrero, J. M. Feliu, *J. Solid State Electrochem.* **2007**, *11*, 1531–1539.
[68] N. Marković, P. Ross Jr, *Surf. Sci. Rep.* **2002**, *45*, 117–229.
[69] N. Marković, B. Grgur, C. Lucas, P. Ross, *J. Phys. Chem. B* **1999**, *103*, 487–495.
[70] M. Heinen, Y. Chen, Z. Jusys, R. J. Behm, *Electrochim. Acta* **2007**, *52*, 5634–5643.
[71] A. A. Topalov, A. R. Zeradjanin, S. Cherevko, K. J. Mayrhofer, *Electrochem. Commun.* **2014**, *40*, 49–53.
[72] S. Brankovic, N. Marinkovic, J. Wang, R. Adžić, *J. Electroanal. Chem.* **2002**, *532*, 57–66.
[73] N. Marinkovic, M. Vukmirovic, R. Adzic, *Modern Aspects of Electrochemistry*, Springer, **2008**, pp. 1–52.
[74] M. S. Rau, M. R. G. de Chialvo, A. C. Chialvo, *J. Power Sources* **2012**, *216*, 464–470.
[75] H. Hoster, R. Behm, *Fuel Cell Catalysis: A Surface Science Approach*, Wiley, Hoboken, NJ **2009**, p. 465.
[76] N. Lebedeva, M. Koper, J. v. Feliu, R. Van Santen, *J. Phys. Chem. B* **2002**, *106*, 12938–12947.
[77] J. Inukai, D. A. Tryk, T. Abe, M. Wakisaka, H. Uchida, M. Watanabe, *J. Am. Chem. Soc.* **2013**, *135*, 1476–1490.
[78] W. Chen, N. Uwitonze, F. He, M. M. Sartin, J. Cai, Y.-X. Chen, *J. Energy Chem.* **2021**, *56*, 412–419.
[79] Z. Jusys, J. Kaiser, R. J. Behm, *Phys. Chem. Chem. Phys.* **2001**, *3*, 4650–4660.
[80] P. K. Dahlstrøm, D. A. Harrington, F. Seland, *Electrochim. Acta* **2012**, *82*, 550–557.
[81] D. Zhang, O. Deutschmann, Y. Seidel, R. J. Behm, *J. Phys. Chem. C* **2011**, *115*, 468–478.

[82] T. Fuchs, V. Briega-Martos, J. O. Fehrs, C. Qiu, M. Mirolo, C. Yuan, S. Cherevko, J. Drnec, O. M. Magnussen, D. A. Harrington, *J. Phys. Chem. Lett.* **2023**, *14*, 3589–3593.
[83] L. Jacobse, V. Vonk, I. T. McCrum, C. Seitz, M. T. Koper, M. J. Rost, A. Stierle, *Electrochim. Acta* **2022**, *407*, 139881.
[84] O. Alves, H. Hoster, R. Behm, *Phys. Chem. Chem. Phys.* **2011**, *13*, 6010–6021.
[85] A. K. Engstfeld, S. Weizenegger, L. Pithan, P. Beyer, Z. Jusys, J. Bansmann, R. J. Behm, J. Drnec, *Electrochim. Acta* **2021**, *389*, 138350.
[86] I. Martens, R. Chattot, M. Rasola, M. V. Blanco, V. Honkimaki, D. Bizzotto, D. P. Wilkinson, J. Drnec, *ACS Appl. Energy Mater.* **2019**, *2*, 7772–7780.
[87] Z. Jusys, R. Behm, *J. Phys. Chem. B* **2001**, *105*, 10874–10883.
[88] T. Shirasawa, T. Masuda, W. Voegeli, E. Arakawa, C. Kamezawa, T. Takahashi, K. Uosaki, T. Matsushita, *J. Phys. Chem. C* **2017**, *121*, 24726–24732.
[89] T. Iwasita, *Handbook of Fuel Cells–Fundamentals, Technology and Applications*, Vol. *2*, Wiley, Hoboken, NJ **2003**, pp. 603–624.
[90] Y. X. Chen, A. Miki, S. Ye, H. Sakai, M. Osawa, *J. Am. Chem. Soc.* **2003**, *125*, 3680–3681.
[91] Yan, Q.-X. Li, S.-J. Huo, M. Ma, W.-B. Cai, M. Osawa, *J. Phys. Chem. B* **2005**, *109*, 7900–7906.
[92] K. Kopatzki, Sauerstoffadsorption, Oxidbildung und Homoepitaxie auf Ni(100) Oberflächen - eine Untersuchung mit dem Rastertunnelmikroskop. Ph.D. thesis, University München, Munich **1994**.
[93] H. Hoster, A. Bergbreiter, P. M. Erne, T. Hager, H. Rauscher, R. J. Behm, *Phys. Chem. Chem. Phys.* **2008**, *10*, 3812–3823.
[94] M. L. Foresti, A. Pozzi, M. Innocenti, G. Pezzatini, F. Loglio, E. Salvietti, A. Giusti, F. D'Anca, R. Felici, F. Borgatti, *Electrochim. Acta* **2006**, *51*, 5532–5539.
[95] J. Drnec, T. Zhou, S. Pintea, W. Onderwaater, E. Vlieg, G. Renaud, R. Felici, *J. Appl. Crystallogr.* **2014**, *47*, 365–377.

Manuscript received: November 20, 2024
Revised manuscript received: March 7, 2025
Accepted manuscript online: March 9, 2025
Version of record online: April 21, 2025